ResearchGate

See discussions, stats, and author profiles for this publication at: https://www.researchgate.net/publication/243374595

Local Structure of Nanocrystalline Ru 1− x Ni x O 2−δ Dioxide and Its Implications for Electrocatalytic Behavior—An XPS and XAS Study

ARTICLE *in* THE JOURNAL OF PHYSICAL CHEMISTRY C · DECEMBER 2009

Impact Factor: 4.77 · DOI: 10.1021/jp904935e

CITATIONS
10

READS
34

9 AUTHORS, INCLUDING:

Kateřina Macounová
Academy of Sciences of the Czech Republic
29 PUBLICATIONS **565** CITATIONS
SEE PROFILE

Marina Makarova
Institute of Physics ASCR
51 PUBLICATIONS **327** CITATIONS
SEE PROFILE

Sanjeev Mukerjee
Northeastern University
227 PUBLICATIONS **7,546** CITATIONS
SEE PROFILE

Petr Krtil
Academy of Sciences of the Czech Republic
78 PUBLICATIONS **1,207** CITATIONS
SEE PROFILE

Available from: Petr Krtil
Retrieved on: 01 February 2016

Local Structure of Nanocrystalline $Ru_{1-x}Ni_xO_{2-\delta}$ Dioxide and Its Implications for Electrocatalytic Behavior—An XPS and XAS Study

V. Petrykin,[†] Z. Bastl,[†] J. Franc,[†] K. Macounova,[†] M. Makarova,[†] S. Mukerjee,[‡] N. Ramaswamy,[‡] I. Spirovova,[†] and P. Krtil*,[†]

J. Heyrovsky Institute of Physical Chemistry, Academy of Sciences of the Czech Republic, v.v.i, Dolejskova 3, 18223 Prague, Czech Republic, and Depratment of Chemistry and Chemical Biology, Northeastern University, 360 Huntington Ave., Boston, Massachusetts

Received: May 27, 2009; Revised Manuscript Received: September 30, 2009

Chemical composition, crystal structure, as well as short-range atomic arrangement of nanocrystalline $Ru_{1-x}Ni_xO_{2-\delta}$ oxides with x ranging between 0 and 0.3 were studied using energy dispersive X-ray spectroscopy (EDX), X-ray photoelectron spectroscopy (XPS), and X-ray absorption spectroscopy (XAS). The prepared materials form single-phase nanocrystals with rutile structure. Regardless of the chemical composition, the surface of $Ru_{1-x}Ni_xO_{2-\delta}$ oxides is Ni-enriched with respect to overall chemical composition. According to both XPS and XANES, the oxidation state of Ru remains +4 in the studied materials. Ni ions are present in both divalent and trivalent states with the fraction of trivalent ions decreasing with increasing Ni content. The refinement of local structure using EXAFS data based on Ru−K and Ni−K edge absorption spectra shows that Ru preserves local arrangement characteristic for ruthenium dioxide. The incorporated Ni shows a tendency to form clusters within a rutile structure for low Ni concentration. At high Ni content, the architecture of the Ni-rich defects resembles architecture of shear planes in oxygen-deficient rutile. These Ni-rich regions likely manifest themselves on the surface as line or plane defects, which are the most likely structural features active in the electrocatalytic processes.

Introduction

Electrochemical behavior of oxygen is one of the major challenges of current electrocatalytic research. Both the oxygen reduction, such as in the context of the low-temperature polymer electrolyte fuel cells and the oxygen evolution, in the context of water electrolysis, represent the step that kinetically limits the performance of the intended practical applications. While the oxygen reduction proceeds on all chemical types of surfaces, including metals, oxides, or sulfides, the oxygen evolution takes place preferentially on oxide-type surfaces. Due to the electrocatalytic nature of both processes, the electrode material plays a substantial role in control of the total electrochemical activity toward oxygen evolution and in the control of its mechanism. The conductive oxides with rutile structure, namely RuO_2 and IrO_2, are arguably the best man-made electrocatalysts for electrochemical oxygen evolution.[1] The oxygen evolution on these surfaces is often formally viewed as a formation of the instable RuO_3 or IrO_3, which decompose to the stable oxide and oxygen. This process is, however, of a more complex nature and involves substantial rearrangement of the MeO_6 (Me = Ru or Ir) octahedra,[2,3] as reported earlier using isotope labeling experiments, which showed oxygen transfer between the material of the electrode and solution-born species. In the case of other oxides, e.g., of surface oxides of platinum or gold, the formation of which precedes the oxygen evolution, such oxygen transfer reactions are not reported to occur.[4]

Recent reports on the oxygen evolution activity of nanocrystalline ruthenium based oxides with rutile structure showed that the activity toward oxygen evolution can be modified by controlling the shape of the nanocrystals[5,6] or by the substitution of the Ru in the rutile structure by other transition metals.[5,7−14] In contrast to the isovalent substitution [e.g., with Ti(IV)[11,15,16] or Ce(IV)[10]], when one expects a wide solubility range and single-phase character of the prepared materials, the substitution with, for example, Fe,[12] Co,[7] and Ni[13,14] leads to formation of the single-phase oxides with rutile structure only if solution-based low-temperature synthetic approaches are employed. All such materials are, however, of metastable character and decompose if annealed even at moderate temperatures (600−800 °C).[7,13] As was shown for the case of Ni- and Fe-substituted ruthenium oxides, the incorporation of the doping cation significantly alters the electrocatalytic behavior of the electrode material in anodic processes. The presence of the doping cation generally improves the activity of the doped oxides toward oxygen evolution;[14] it also significantly alters the selectivity of the oxide surface.[13] A simple structural model explaining the observed effects of the heterovalent substitution was proposed on the basis of the data gathered for Ni-doped RuO_2.[13,14] The model assumes that the doping cations affect the electrocatalytic behavior of the materials via cation−cation interactions and proposes clusters involving first two coordination shells as the model of active sites.[13] The experimental electrocatalytic activity and selectivity data can be rationalized in terms of variations of the numbers and types of active sites present.[13] It needs to be noted that the proposed structure of such active sites does not need to reflect the actual one and has yet to be demonstrated. Such a demonstration has been hindered mainly by the lack of the knowledge on the structure of this type of oxide systems on the local level.

The issue of the active site structure is addressed in this paper, which summarizes the results of spectroscopic investigations

* To whom correspondence should be addressed. E-mail: petr.krtil@jh-inst.cas.cz.
[†] Academy of Sciences of the Czech Republic.
[‡] Northeastern University.

10.1021/jp904935e © 2009 American Chemical Society
Published on Web 12/03/2009

of $Ru_{1-x}Ni_xO_{2-\delta}$ ($0<x<0.3$) by a combination of X-ray photoelectron spectroscopy (XPS) and X-ray absorption spectroscopic techniques. The XPS and short-range structure data from EXAFS are related to results of electrochemical investigations of the oxygen evolution on $Ru_{1-x}Ni_xO_{2-\delta}$ materials.

Experimental Section

The $Ru_{1-x}Ni_xO_{2-\delta}$ samples were prepared by the procedure described previously[13,14] using a coprecipitation method combined with solvothermal aging. The starting solutions of ruthenium(III) nitrosylnitrate (98%, Alpha Aesar) and nickel(II) nitrate hexahydrate in a mixture of ethanol and propane-2-ol (1:1) (both Aldrich, ACS grade) were precipitated with aqueous solution of tetramethylammonium hydroxide (25% Alpha Aesar).[13] These starting solutions were characterized by set Ru:Ni ratio of 49:1, 19:1, 9:1, 4:1, 3:1, and 7:3. The precipitation procedure led to a formation of amorphous precursors that were aged in a PTFE-lined stainless steel autoclave at 100 °C for 40 h. The washed and filtered powders were treated with hydrogen peroxide (1%), dried in air, and annealed at 400 °C in air for 1 h to obtain nanocrystalline materials. The crystallinity and phase purity of the prepared samples were confirmed using a Bruker D8 Advance powder X-ray diffractometer with Vantec-1 detector and Cu Kα radiation. The bulk chemical composition of the prepared materials was analyzed using X-ray energy dispersive spectroscopy on a Hitachi S4800 scanning electron microscope (SEM) equipped with a Nanotrace EDX detector (Thermo Electron).

The short-range structure was assessed by means of X-ray absorption spectroscopy (XAS). X-ray near-edge absorption spectra (XANES) as well as extended X-ray absorption fine structure (EXAFS) data were measured on pellets containing approximately 40 mg of $Ru_{1-x}Ni_xO_{2-\delta}$ in 200 mg of boron nitride (ACS grade, Wako Chemicals). The XANES and EXAFS spectra were measured at the Photon Factory synchrotron of the High Energy Accelerator Organization (KEK) in Tsukuba, Japan. The spectra were measured in transmission mode on Ru K edge [beamline AR-NW10A; Si(311) monochromator] and Ni K absorption edge [BL-12C beamline; Si(111) monochromator]. The Ni edge XAS spectra of the material with x equal to 0.05 were acquired in fluorescence mode using a Lytle detector. Ru K scans extended to 20 $Å^{-1}$ and Ni K data were limited to 15 $Å^{-1}$. Each spectrum was recorded at four different scanning step sizes: pre-edge region from 500 to 50 eV was scanned in 6.5 eV steps to enable background subtraction; in the 50 eV pre-edge and 100 eV postedge range, the step size of 0.4−0.5 eV was used to acquire the XANES part of the spectra, while 2.5−3.0 and 7.0 eV scanning step was maintained in the postedge regions of 100−500 and above 500 eV, respectively.

All data handling prerequisite to the local structure refinement of the extended X-ray absorption fine structure (EXAFS) functions (i.e., normalization, smoothing and background subtraction, the Fourier transforms of the spectra and windowing) was done in the IFEFFIT software package.[17] The photoelectron wave vector k for the Fourier transform of spectra was kept within the range of $k = 3-18$ $Å^{-1}$ for Ru-EXAFS and $k = 3-14$ $Å^{-1}$ for Ni-EXAFS. The k-weighting factor of 2 was applied. For presenting EXAFS functions in the R-space (real space) the ranges of $R = 1-6$ and $1-4$ Å were used for Ru and Ni EXAFS, respectively.

For analysis of local structure of the $Ru_{1-x}Ni_xO_{2-\delta}$ ($x = 0.0$, 0.05, 0.10, and 0.30) materials, full-profile refinement of the EXAFS spectra by nonlinear least-squares (NLLS) minimization in the R-space with k-weighting factor equal to 2 was carried out using the Artemis NLLS module of the IFEFFIT package. The theoretical model was generated using the FEFF6.2 library with structural parameters of an ideal RuO_2 rutile crystal.[18]

The refinement procedure consisted of three stages. In the first stage, the initial structure was allowed to expand isotropically and the values of amplitude, phase shift (ΔE_0), and Debye−Waller factors for cations and anions were refined. In the second stage, the isotropic expansion/contraction was kept only for the first metal−oxygen coordination shell and for the other core metal−oxygen distances, while the distances from the core cation to other cations were allowed to change independently. During the final stage of the refinement, the results for the model with the minimal set of single-scattering paths were compared with the refinement of the model, which additionally included collinear multiple scattering paths and scattering events with the contribution lower than 7% to identify the reasonably limited set of the paths constituting the model needed for providing unique fits of experimental spectra.

In the refinement of Ni-EXAFS data for $Ru_{1-x}Ni_xO_{2-\delta}$ ($x = 0.05$, 0.10) samples were both structural models refined simultaneously by using EXAFS functions for both materials applying constraints onto the Ru−Ni interatomic distances and keeping identical Debye−Waller factors for similar type of atoms in both clusters, while amplitude and phase shift correction parameters were refined independently for each composition. Along with these constraints, it was assumed that the differences in EXAFS functions of these materials are primarily due to the different Ru and Ni occupancies in the metal sites around the core metal. Although Artemis does not allow direct refinement of coordination numbers, metal site occupancies in the two nearest coordination shells were evaluated by introducing and refinement of an additional parameter, which provides a link between the amplitude and the degeneracy of each metal site.

The chemical analysis of the $Ru_{1-x}Ni_xO_{2-\delta}$ surfaces was based on X-ray photoelectron spectroscopy (XPS). The photoelectron spectra of the samples were measured using an ESCA310 (Scienta, Sweden) electron spectrometer equipped with a high power rotating anode, wide-angle quartz crystal monochromator and a hemispherical electron analyzer operated in a fixed transmission mode. Monochromatic Al Kα radiation was used for electron excitation. The resolution of the instrument was 0.30 eV using the silver Fermi edge. The energy scale of the spectrometer was calibrated to the Au $4f_{7/2}$ binding energy fixed at 84.0 eV. The spectra were recorded at room temperature. The spectra of Ru 3d, Ru3p, O 1s, and Ni 2p photoelectrons were measured. The electron takeoff angle was 90° with respect to the macroscopic sample surface. The samples were good electrical conductors, and consequently, the surface static charging was not observed. The pressure of residual gases in the analyzer chamber during spectra acquisition was 2×10^{-9} mbar. The accuracy of the measured electron energies was ±0.1 eV. The spectra were curve fitted after subtraction of Shirley background[19] using Gaussian−Lorentzian line shape and a nonlinear least-squares algorithm. For fitting of Ru 3d spectra asymmetrical line shapes were used. Quantification of the surface elemental concentrations was accomplished by correcting photoelectron peak intensities for their cross sections,[20] analyzer transmission function, and dependence of inelastic mean free paths of electrons on their kinetic energy.

Results and Discussion

XRD. The X-ray diffraction patterns of the synthesized $Ru_{1-x}Ni_xO_{2-\delta}$ oxides are shown in Figure 1. The diffraction

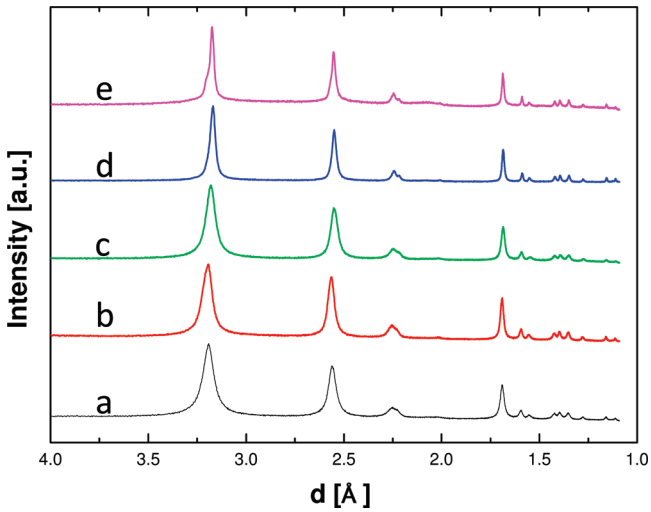

Figure 1. X-ray diffractograms of $Ru_{1-x}Ni_xO_{2-\delta}$ oxides with x equal to 0.05 (a), 0.10 (b), 0.15 (c), 0.20 (d), and 0.30 (e).

peaks for all the prepared materials can be identified as belonging to a single-phase compound with a rutile structure having peak positions close to that of RuO_2. Flat background and absence of a diffuse scattering indicate the absence of an amorphous phase coexisting with the nanocrystalline $Ru_{1-x}Ni_xO_{2-\delta}$ oxides. Even for a high Ni concentration of $x = 0.30$, we could not identify additional reflections, which may appear due to ordering of Ni in the lattice or the presence of ordered oxygen vacancies. The measured powder diffraction patterns show a shift of the reflection positions for different amounts of Ni doping, indicating a change of the unit cell volume. Refinement of crystal structures by the Rietveld method revealed continuous decrease of the unit cell volume with the increase in Ni content (see Supporting Information). This trend indicates Ni substitution into the Ru site in the whole range of $0 < x < 0.3$. In fact, one should not expect a significant variation of lattice parameters vs Ni concentration due to a very small difference in the ionic radii of Ni^{2+} (0.69 Å), Ni^{3+}(0.56 Å), and Ru^{4+} (0.62 Å) in the octahedral environment.[21] It needs to be stressed that the overall decrease of the unit cell volume results from opposite trends in the individual lattice parameters a and c. (The unit cell parameter along the a axis increases and the unit cell parameter along the c axis decreases.) Such a variation of lattice constants may reflect different ion−ion interactions along the a and c axes of the structure resulting from the heterovalent substitution. These characteristic features of the presented diffraction data are compatible in general with the discussions adopted in ref 13 assuming a homogeneous distribution of Ni in the lattice.

The results of the chemical analysis by energy dispersive X-ray spectroscopy (EDX) are summarized in Figure 2. One may notice that the content of Ni in the prepared samples continuously increases with increase of Ni concentration in the starting solution. The EDX analysis carried out after electrochemical experiments reflects thechemical stability of the prepared $Ru_{1-x}Ni_xO_{2-\delta}$ phases. The prepared materials seem to be reasonably stable under (rather harsh) conditions of the electrochemical experiments (chloride-containing acid media, oxidative potentials of oxygen, and chlorine evolution) as long as the nominal Ni content does not exceed $x = 0.1$ (see Figure 2). At higher nominal Ni contents, the observed difference between the actual bulk Ni content before and after electrochemical experiments clearly shows a decrease of the total Ni content connected with anodic processes.

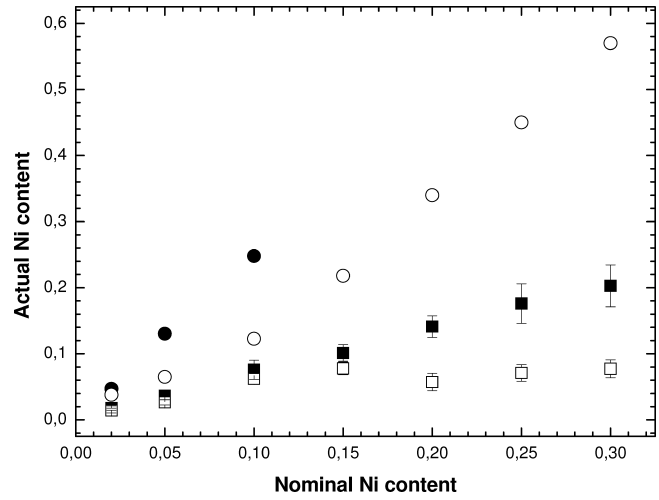

Figure 2. Actual Ni content as a function of the nominal Ni content in the as prepared electrodes (solid symbols) and in the electrode after electrocatalytic oxygen evolution in acid media (red open symbols) determined by EDX (squares) and XPS (circles) analyses.

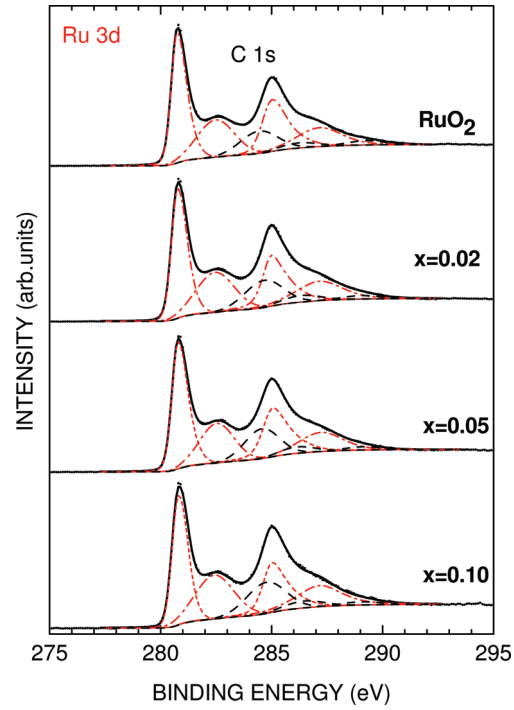

Figure 3. Fitted spectra of Ru 3d−C 1s photoelectrons taken from $Ru_{1-x}Ni_xO_{2-\delta}$ electrodes with variable Ni content after electrocatalytic oxygen evolution in acid media.

XPS. The spectra of Ru 3d, Ni 2p, and O 1s photoelectrons of the prepared $Ru_{1-x}Ni_xO_{2-\delta}$ oxides are shown in Figures 3−6. It needs to be noted that the Ru 3d photoelectron spectra overlap with spectra of C1s photoelectrons of the adventitious carbon (see Figure 3). The intensity of the latter was subtracted from the fitted Ru 3d−C 1s spectra before using the Ru 3d intensities for calculation of the surface stoichiometry of the samples. For the purpose of comparison, the intensities of Ru 3p spectra were also used for calculation of the surface composition and consistent results were obtained. The surface stoichiometry of the samples calculated from integrated intensities of photoelectron spectra is summarized along with EDX data in Figure 2 and Table 1.

Regardless of the projected Ni content, the XPS data indicate an apparent excess of the Ni at the oxides' surface with respect

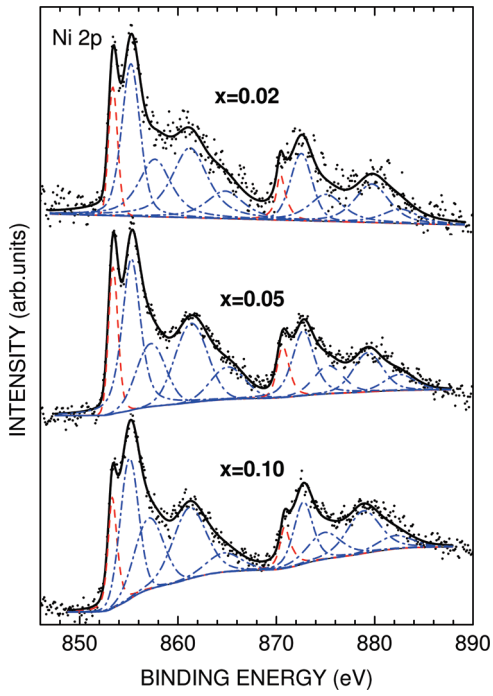

Figure 4. Fitted spectra of Ni 2p photoelectrons taken from $Ru_{1-x}Ni_xO_{2-\delta}$ electrodes with variable Ni content after electrocatalytic oxygen evolution in acid media.

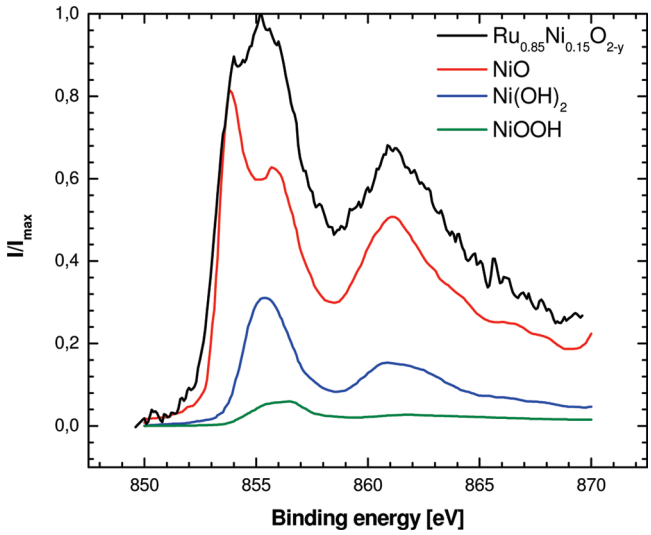

Figure 5. A comparison of the experimental Ni 2p photoelectron spectrum of $Ru_{0.85}Ni_{0.15}O_{2-\delta}$ with those of NiO, $Ni(OH)_2$, and NiO(OH).

to the corresponding bulk composition. Relative underrepresentation of Ru on the surface of binary oxides was well documented in the literature[22−24] and was ascribed to both phase separations near the surface as well as to a specific screening effects. Although the ruthenium remains to be a major component in the superficial layers of all oxides with $x < 0.25$, at higher Ni contents the surface starts to be slightly dominated by Ni. The high Ni surface excess in the as received materials was not, however, confirmed by structure sensitive X-ray absorption spectroscopy (XAS) (see below). The surface Ni content drops according to the XPS data after exposure of the electrodes to acid media in electrochemical experiments. This behavior may be interpreted in terms of selective Ni leaching from the surface. Such a mechanism is in agreement with the EDX data for materials with high nickel content ($x > 0.10$). It contradicts,

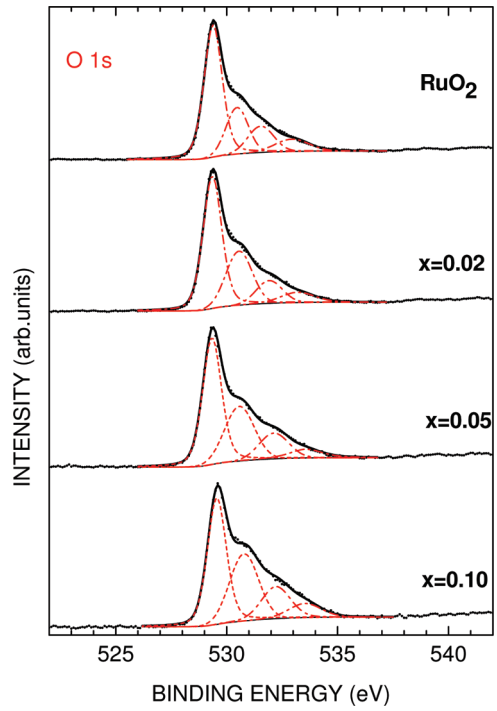

Figure 6. Fitted spectra of O 1s photoelectrons taken from $Ru_{1-x}Ni_xO_{2-\delta}$ electrodes with variable Ni content after electrocatalytic oxygen evolution in acid media.

TABLE 1: XPS-Based Surface Chemical Composition of the $Ru_{1-x}Ni_xO_{2-\delta}$ Materials before and after Electrochemical Treatment

	XPS	
nominal composition	as received	after electrochemistry
$Ru_{0.98}Ni_{0.02}O_{2-\delta}$	$Ru_{0.954}Ni_{0.046}O_{2.60}C_{2.50}$	$Ru_{0.962}Ni_{0.038}O_{2.23}C_{2.10}$
$Ru_{0.95}Ni_{0.05}O_{2-\delta}$	$Ru_{0.870}Ni_{0.13}O_{2.46}C_{1.99}$	$Ru_{0.935}Ni_{0.065}O_{2.33}C_{2.04}$
$Ru_{0.90}Ni_{0.10}O_{2-\delta}$	$Ru_{0.752}Ni_{0.248}O_{2.32}C_{2.075}$	$Ru_{0.872}Ni_{0.128}O_{2.78}C_{1.99}$

however, the EDX results obtained for materials with low nominal Ni content ($x < 0.10$) when the EDX does not confirm any decrease of the total Ni content. It has to be stressed that studied electrodes are composed of randomly oriented nanoparticles the characteristic particle size of which (ca. 20 nm) is comparable with the mean free path of the photoelectrons. In this respect, the XPS spectra do not reflect just a surface concentration, but in fact probe significant fraction of the bulk of individual nanocrystals. This makes an agreement between XPS and EDX results of particular importance.

The apparent conflict between XPS and EDX composition data can be resolved by acknowledging the fact that the adventitious carbon present on the materials surface and which screens produced photoelectrons does not need to be distributed homogeneously on the surface but may be preferentially localized in Ru or Ni environment. As follows from the literature, Ni oxides do not show substantial affinity for carbonaceous species;[25] the RuO_2, on the other hand, adsorbs readily the oxygen-containing carbonaceous species.[26] The screening effect of the adventitious carbon localized on Ru may lower the detected intensity of Ru photoelectrons, resulting in apparent Ni enrichment of the surface.

The screening effect of adventitious carbon on the XPS data of $Ru_{1-x}Ni_xO_{2-\delta}$ may be altered in electrochemical experiments since the experimental conditions allow for electrochemical removal of adventitious carbon. Such a decrease of the adventitious carbon content is reflected in data presented in Table 1.

The observed decrease in the Ni:Ru ratio calculated from the XPS spectra of materials after electrochemical experiments may, therefore, result from removal of adventitious carbon rather than from the Ni leaching. This model also suggests that the surface Ni content might be apparently overestimated and does not need to reflect the actual surface composition. It is worth mentioning that the obtained oxygen content exceeds the one expected by simple stoichiometric relations and undergoes complex changes during electrochemical experiments. This can be attributed to the presence of surface hydroxyl groups and adsorbed water (see Figure 6), the content of which may be strongly affected by the materials' history.

In addition to general information about quantitative chemical composition of the surface, the XPS spectra reflect also the distribution of the electron density on the absorbing atoms; hence, it can provide the information on the distribution of both Ru and Ni oxidation states near the surface. The X-ray photoelectron spectra of all measured elements are of complex character reflecting the chemistry of the $Ru_{1-x}Ni_xO_{2-\delta}$ oxides. A detailed analysis of the Ru and Ni photoelectron spectra will be given separately.

Ru 3d XP Spectra. The spectra of Ru 3d photoelectrons of Ni substituted oxides do not differ from that of pure RuO_2 (Figure 3.) and are not affected by electrochemical treatment of samples. The spectrum of Ru $3d_{5/2}$ photoelectrons consists of a main peak located at 280.7 eV and a broad satellite peak centered at 282.4 eV. The origin of the second peak has been the source of discussions in the literature. Some of the authors assigned it to Ru^{6+} present on the sample surface,[27,28] while others have attributed it to final state effects in photoemission. Recently, it has been proposed that the satellite peak is due to plasmon excitation.[29,30] The reduction of RuO_2 sample during spectra measurements reported in the literature[31] was not observed under experimental conditions used in the present work.

The assignment of the satellite peak located at 282.4 eV is of particular importance to understand the redox chemistry and eventually the electrocatalytic properties of Ni-doped ruthenium oxides. An intuitive approach suggests that there are in principle two modes to compensate for expected decrease of positive charge in the cationic sublattice due to the incorporation of the Ni. One can assume formation of the vacancies in the oxygen sublattice. Alternatively, one can also anticipate a partial stabilization of Ru oxidation state higher than +4. The latter hypothesis might be compatible with the assignment of the satellite peak at 282.4 eV to Ru^{6+}. The fact that the fraction of the Ru in such an oxidation state shows a very weak dependence on the actual surface chemical composition speaks, however, against this assignment.

Ni 2p XP Spectra. The interpretation of Ni 2p photoelectron spectra encounters similar difficulties as that of Ru 3d photoelectron spectra. The E_b interval between 850 and 890 eV features a narrow peak at 853.3 eV and two broad, structured peaks located at 855.3 and 861 eV (see Figure 4). The assignment and quantification of different chemical states of nickel in the measured materials are difficult tasks due to the complex and multiplet structure of the Ni 2p photoelectron spectra, details of which depend on the metal ion environment.[32] The nature of the peaks suggests variability of the Ni oxidation state as well as of its coordination. Since the effects of oxidation state and coordination are difficult to separate, we plot Ni 2p XP spectra of reference compounds such as nickel(II) oxide, nickel(II) hydroxide, and nickel(III) oxohydroxide along with the typical spectrum of the $Ru_{1-x}Ni_xO_{2-\delta}$ (see Figure 5). As follows from Figure 5, the spectra of the reference compounds can reproduce the most important features of the Ni 2p spectra. It suggests that the Ni^{2+} oxidation state dominates in the surface layers of the synthesized samples with possible admixture of small amounts of Ni^{3+}, the fraction of which seems to decrease with increasing total amount of Ni. The distribution of oxidation states of Ni can be at least in principle determined by a more rigorous approach based on Gupta and Sen calculations[33] utilizing the Ni free ion states.[34] On the other hand, the use of such a sophisticated approach lacks justification without detailed information on the local environment of Ni in the $Ru_{1-x}Ni_xO_{2-\delta}$ oxides. For example, using Gupta−Sen multiplets for sample containing Ni^{2+} and Ni^{3+} valence states, the spectrum of Ni 2p electrons should be fitted by 20 overlapping components, which makes the results of such fit doubtful even if additional constrains are applied.

O 1s XP spectra. The spectra of O 1s photoelectrons depicted in Figure 6 are similar for RuO_2 and Ni-containing mixed oxides. They consist of four components located at 529.3, 530.7, 532.0, and 533.3 eV. The first peak can be attributed to O^{2-} species. The intensity of this peak relative to intensity of Ru 3d peak does not depend on the Ni concentration in the sample. The second component (530.6 eV) can be assigned to OH groups. The intensity of this component increases with increasing amount of Ni in the sample; the remaining two peaks (at 532.0 and 533.3 eV) can be attributed to oxygen in adsorbed water and adsorbed CO_2 and/or oxygen in carboxyl groups.[35]

X-ray Absorption Spectroscopy

The limited ability of the XPS to interpret the redox composition of the sample surface in structural terms prompts a complementary approach which is both sensitive to an average oxidation state of present transition metals and to their local environment. This complementary information can be provided by X-ray absorption spectroscopy (XAS).

XANES. The typical XANES spectra of the $Ru_{1-x}Ni_xO_{2-\delta}$ samples measured on Ru and Ni K absorption edges are shown in Figure 7a,b. The absorption edges (determined from the derivatives of the normalized spectra) were used to estimate the formal average oxidation states of both ruthenium and nickel in $Ru_{1-x}Ni_xO_{2-\delta}$ oxides. As follows from Figure 7a, all $Ru_{1-x}Ni_xO_{2-\delta}$ oxide samples have, regardless of the actual Ni content, the position of the Ru absorption K edge E_0 close to 22 125 ± 3 eV. A comparison of E_0 values of the $Ru_{1-x}Ni_xO_{2-\delta}$ with the absorption edges of reference Ru compounds (see inset to Figure 7a) yields the formal oxidation state of Ru in synthesized materials as 4.3 ± 1. The average oxidation state value cannot be distinguished from that of the RuO_2 and shows very weak dependence on the overall chemical composition of $Ru_{1-x}Ni_xO_{2-\delta}$ oxides. This result clearly favors the assignment of the satellite peak in the Ru 3d XPS spectra to a plasmon excitation.

In a similar manner, the Ni K edge XANES spectra of $Ru_{1-x}Ni_xO_{2-\delta}$ oxides with $x > 0.10$ show weak dependence on the actual nickel content. The actual value of E_0 in these materials equals to 8338 eV, which is positive of that of nickel oxide (see Figure 7b). The E_0 measured for the sample with $x = 0.05$ is located at 8340 eV, which is the most positive value for the series of $Ru_{1-x}Ni_xO_{2-\delta}$ materials. In contrast to the XANES spectra measured on Ru edge, it was not possible to use E_0 values for Ni edge of known standards to estimate the formal oxidation state of Ni in $Ru_{1-x}Ni_xO_{2-\delta}$ samples. This fact has to be attributed mainly to the relative lack of convenient well-defined standards with oxidation state of Ni higher than

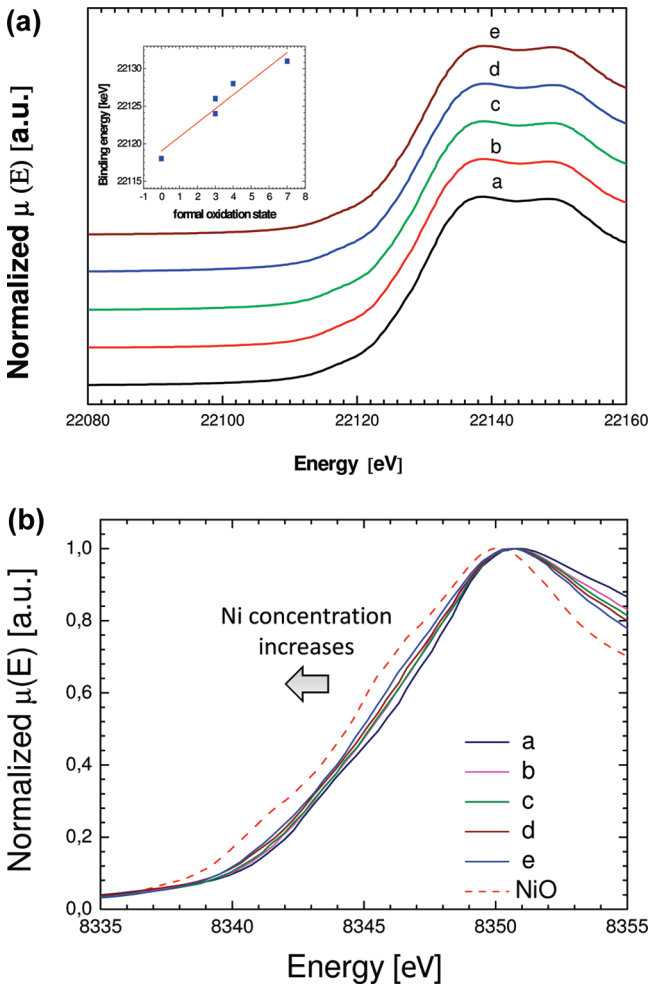

Figure 7. (a) XANES part of the Ru K edge X-ray absorption spectra of $Ru_{1-x}Ni_xO_{2-\delta}$ oxides with x equal to 0.05 (a), 0.10 (b), 0.15 (c), 0.20 (d), and 0.30 (e). The inset shows the calibration of the absorption edge position as a function of formal oxidation state of ruthenium. (b) XANES part of the Ni K edge X-ray absorption spectra of $Ru_{1-x}Ni_xO_{2-\delta}$ oxides with x equal to 0.05 (a), 0.10 (b), 0.15 (c), 0.20 (d), and 0.30 (e).

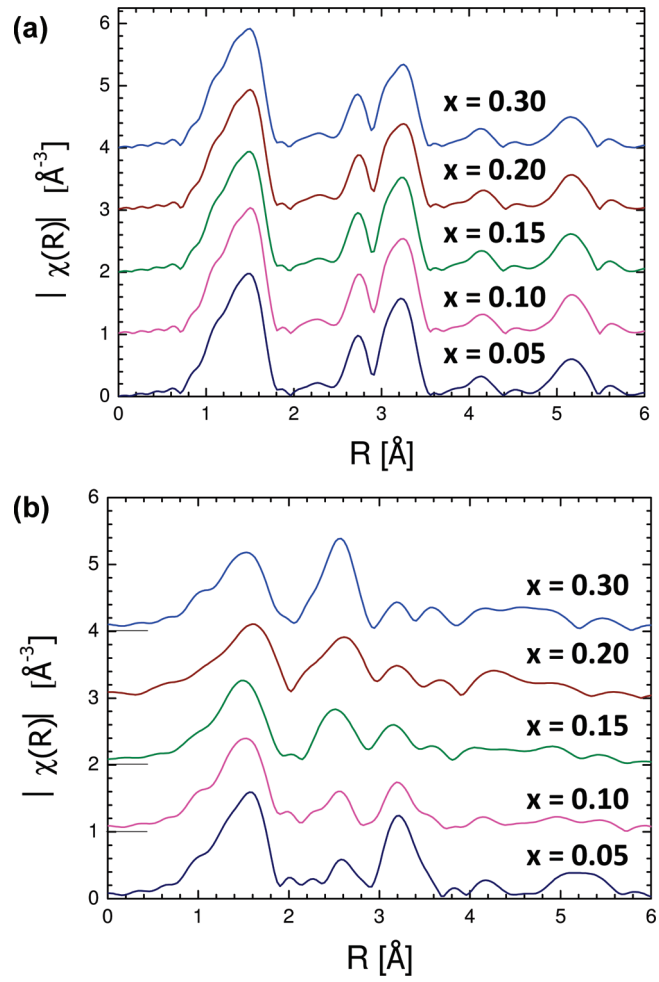

Figure 8. (a) k^2-Normalized Fourier transformed EXAFS functions calculated from the Ru K edge X-ray absorption spectra of $Ru_{1-x}Ni_xO_{2-\delta}$ oxides with variable nickel content. The curve assignments are given in the figure legend. Correction for the phase shift is not applied. (b) k^2-Normalized Fourier transformed EXAFS functions calculated from the Ni K edge X-ray absorption spectra of $Ru_{1-x}Ni_xO_{2-\delta}$ oxides with variable nickel content. The curve assignments are given in the figure legend. Correction for the phase shift is not applied.

+2. The weak dependence of the E_0 of the $Ru_{1-x}Ni_xO_{2-\delta}$ on the actual Ni content stresses the need to interpret the XANES spectra in terms of both oxidation state and coordination of the absorbing atom local environment which needs, therefore, to be taken into consideration.

EXAFS. The structural information about local environment of the ruthenium and nickel ions was extracted from the extended X-ray absorption fine structure (EXAFS) data calculated from X-ray absorption spectra for energies higher than 50 eV with respect to E_0. The k^2-normalized Ru and Ni K edge EXAFS functions $\chi(R)$ of $Ru_{1-x}Ni_xO_{2-\delta}$ are plotted in Figure 8a,b. In order to stress the chemical information carried by the EXAFS and to show the complementary character of the short-range order with respect to, for example, diffraction data, we present the results of the EXAFS data refinement in R space. It needs to be noted that the goal of local structure refinement was to find a reasonable structural model rather than to elucidate the precise geometry of an unknown atomic cluster or a molecule. Therefore, only single-scattering paths were included in the refinement, while multiple collinear scattering events were considered only to evaluate the quality of the fit and verify the sensitivity of the refined parameters with respect to the simplifications assumed in the model. In general, it can be said that including multiple-scattering paths improves the quality of the fit; it does not need to lead, however, to a significant improvement in the accuracy of the structural information. The involvement of multiple-scattering paths into the model leads to changes in refined values of bond length parameters on the order of 0.04 Å, which is well below the resolution dictated by the finite range of k values involved in the Fourier transform (20 $Å^{-1}$ in the case of Ru and 14 $Å^{-1}$ in the case of Ni).

Anticipating that the $Ru_{1-x}Ni_xO_{2-\delta}$ oxides are of a single-phase character and conform to the rutile structural model (suggested by the X-ray diffraction data), we should, in principle, expect qualitatively similar EXAFS functions, regardless of the edge energy (Ru or Ni K edge) and sample chemical composition. This anticipation is reasonably met for the EXAFS functions calculated from Ru K edge spectra; the agreement of the EXAFS functions obtained from Ni K edge spectra with that of rutile structure is obtained only in the case of materials with $x \leq 0.1$.

Ru K Edge. The EXAFS functions calculated from the X-ray absorption spectra of the $Ru_{1-x}Ni_xO_{2-\delta}$ acquired on Ru K edge conform to that derived theoretically for ruthenium core atom in crystalline RuO_2 and also agree qualitatively with the experimental data measured for reference RuO_2. The Ru K edge EXAFS functions obtained from measured spectra can be

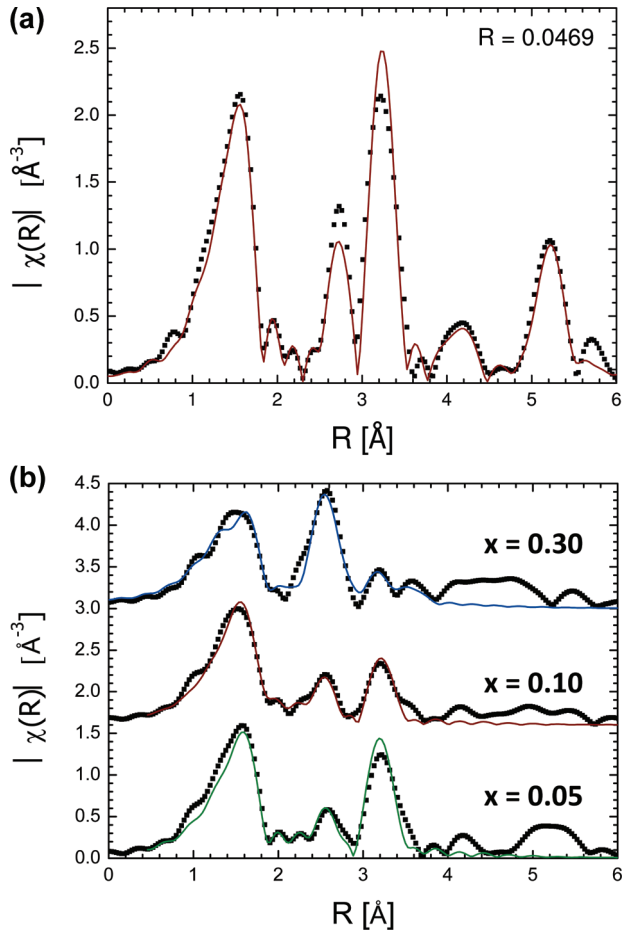

Figure 9. (a) Typical k^2-normalized Fourier transformed EXAFS function calculated from the Ru K edge X-ray absorption spectra of $Ru_{1-x}Ni_xO_{2-\delta}$ (squares) and the best fit (red line) resulting from full profile refinement. The shown spectrum corresponds to material with $x = 0.10$; quality of the fit parameter R is shown in the figure legend. Correction for the phase shift is not applied. (b) Typical k^2-normalized Fourier transformed EXAFS functions calculated from the Ni K edge X-ray absorption spectra of $Ru_{1-x}Ni_xO_{2-\delta}$ (squares) and the best fit (lines) resulting from local structure refinement. The assignments of the curves are shown in the figure legend. Correction for the phase shift is not applied.

satisfactorily fitted with a structural model of rutile crystal within the R range of 1−6 Å (see Figure 9a). The parameters of the fits, namely, the bond lengths and the Debye−Waller factors, are summarized in Table 2a.

The Ru EXAFS functions plotted in R space for materials with different Ni concentration are dominated by the scattering from oxygen atoms directly coordinating the ruthenium atoms. The bonding distance between Ru and O in prepared samples ranges between 1.94 and 1.98 Å. These values seem to be little dependent on the actual Ni content and agree well with the values expected for a bond length between tetravalent ruthenium and oxygen.[37] It ought to be noted that the actual EXAFS data do not distinguish between axial and equatorial Ru−O bond distances, which ought to differ according to the structural model by ca. 0.04 Å. The theoretically predicted difference of these two bond lengths (0.04 Å) is, however, comparable with the resolution of the technique.

A significantly weaker signal can be attributed to the two nearest neighbor Ru−Ru positions located approximately 3.1 Å in the direction of the c axis. Both the position and intensity of the peak in EXAFS functions corresponding to the nearest cations (effective scattering path ca. 3.1 Å) do not change with

TABLE 2: Parameters of the EXAFS Refinement of RuO_2 and $Ru_{1-x}Ni_xO_{2-\delta}$

(a) Essential Refined Interatomic Distances and Corresponding Debye−Waller Factors (DW) for RuO_2 Obtained by Fitting the k^2-Normalized EXAFS Function in R Space for Ru K Edge (22 117 eV) X-ray Absorption Spectra

path	coordination number	bond length, Å: ref 19	bond length, Å: refined	DW, Å^2
R factor = 0.0589, k range = 3.3−20 Å^{-1}, R range = 1−6 Å, amplitude = 0.992, E_0 = 0.438 eV				
Ru−O	2	1.9902	1.983(6)	0.0022(8)
	4	1.9279	1.921(5)	
Ru−Ru	2	3.0995	3.109(7)	0.0025(4)
Ru−Ru	8	3.5344	3.544(4)	0.0034(3)
Ru−Ru	4	4.4923	4.490(30)	0.0056(3)
Ru−Ru	8	5.4578	5.469(11)	0.0032(7)
Ru−Ru	8	5.6308	5.695(20)	0.0052(9)

(b) Essential Refined Interatomic Distances, Debye−Waller Factors (DW), and Ru/Ni Site Occupancies in $Ru_{1-x}Ni_xO_{2-\delta}$ ($x = 0.05$, 0.10, and 0.30) Materials Obtained from the k^2-Normalized EXAFS Functions in R Space for Ni K Edge (8333 eV) X-ray Absorption Spectra

path	coordination number	occupancy	bond length, Å	DW, Å^2
$Ru_{1-x}Ni_xO_{2-\delta}$ ($x = 0.05$), R = 0.0374, k range = 3.0−14 Å^{-1}, R range = 1−4 Å, amplitude = 0.652, E_0 = −1.878 eV				
Ni−O	2	1.0	1.937(3)	0.0026(7)
	4	1.0	2.015(9)	0.0026(7)
Ni−Ru	2	1.00	3.060(20)	0.0036(4)
Ni−Ni		0.00	2.941(55)	
Ni−Ru	8	0.77(11)	3.518(13)	0.0036(4)
Ni−Ni		0.23(11)	3.372(5)	0.0036(4)
$Ru_{1-x}Ni_xO_{2-\delta}$ ($x = 0.10$), R = 0.0396, k range = 3.0−14 Å^{-1}, R range = 1−4 Å, amplitude = 0.732, E_0 = −2.02 eV				
Ni−O	2	1.0	2.081(51)	0.0026(7)
	4	1.0	1.966(8)	0.0026(7)
Ni−Ru	2	0.14(44)	3.060(20)	0.0036(4)
Ni−Ni		0.86(44)	2.941(55)	
Ni−Ru	8	0.61(12)	3.518(13)	0.0036(4)
Ni−Ni		0.39(12)	3.372(5)	0.0036(4)
$Ru_{1-x}Ni_xO_{2-\delta}$ ($x = 0.30$), R = 0.020, k range = 3.0−14.5 Å^{-1}, R range = 1−4 Å, amplitude = 0.97, E_0 = −6.26 eV				
Ni−O	CN = 6; isotropic expansion of NiO_6 octahedron		1.824(3)	0.0020(6)
			1.944(3)	
			1.970(3)	
			2.013(3)	
			2.046(3)	
			2.117(3)	
Ni−Ni	1	1.0	2.843(6)	0.0003(6)
Ni−Ru	1	1.0	2.808(10)	0.0043(5)
Ni−Ni	1	1.0	2.96(1)	0.0003(6)
Ni−Ru	1	1.0	3.15(1)	0.0043(5)
Ni−Ni	1	1.0	3.44(1)	0.0003(6)
Ni−Ru	1	1.0	3.52(2)	0.0043(5)
Ni−Ru	1	1.0	3.54(2)	0.0043(5)
Ni−Ni	1	1.0	3.55(1)	0.0003(6)
Ni−Ni	1	1.0	3.60(1)	0.0003(6)
Ni−Ru	1	1.0	4.08(3)	0.0043(5)
Ni−Ru	1	1.0	4.14(3)	0.0043(5)

Ni content. This trend indicates that the cation arrangement along the c axis is preserved in the vicinity of Ru atoms and that the cationic sites along this direction are preferentially occupied with Ru atoms. The subsequent maximum with an effective length between 3.4 and 3.6 Å can be attributed to a confluence of several scattering events dominated by the

scattering from the eight cationic positions with Ru−Ru distance of approximately 3.5 Å. This corresponds to the coordination of core atom by the nearest Ru ions located along the [111] direction of rutile unit cell. In contrast to the first two peaks, the intensity of the signal corresponding to the effective scattering path of ca. 3.5 Å decreases with increasing Ni content. The full width at half-maximum (fwhm) of this peak also shows slight widening with increase of the Ni concentration. The general trend of a decrease of the scattering intensity corresponding to this peak has to be expected due to substitution of Ru with lower Z cation in the structure. The experimentally observed decrease of the EXAFS function peak intensity together with increase of fwhm is, however, significantly bigger than the one predicted theoretically and may indicate increasing structural disorder extending in the material along the [111] direction.

Ni K Edge. In contrast to EXAFS functions calculated from X-ray absorption spectra measured on Ru K edge, those EXAFS functions calculated from spectra measured at the Ni K edge show pronounced variation depending on the actual Ni content.

Refinement of the local structure using Ni edge EXAFS functions of $Ru_{1-x}Ni_xO_2$ with low Ni concentration ($x < 0.05$) shows that the short-range atomic arrangement of the material can be interpreted in terms of Ni substitution into Ru site of a rutile lattice triggering minor structural changes to adjust for a different size and charge of the Ni ion. The refined Ni−O distances (see Table 2b) were 1.94 and 2.01 Å for apical and equatorial oxygen atoms, which are shorter than 2.09 Å, the corresponding bond distances in NiO. The analysis of bond valence sum for Ni ion suggests its oxidation state as 2.45. This result supports the assumption that the oxidation state of Ni in $Ru_{1-x}Ni_xO_{2-\delta}$ is higher than +2, suggested by XANES and XPS data. The refined value of Ni occupancy in the closest metal neighbor lattice positions (along the *c* axis of rutile unit cell) was found to be −0.01; therefore, during the last circle of refinement it was reset to zero and fixed. At the same time, the fraction of Ni atoms in the next metal−metal coordination shell was found to be equal to 0.23. This value significantly exceeds the value expected by assuming statistical distribution of Ni atoms in the material, and it points out to the possible Ni clustering within RuO_2. The occupancy data resulting from the structural refinement, therefore, suggest that the Ni ions are not homogeneously distributed in the structure, as proposed previously,[13] but tend to arrange along the [111] direction or form zigzags, in a way excluding Ni−Ni neighbors along the shortest metal−metal distance. The proposed arrangement can be viewed as an analogue to the arrangement of atoms encountered in the compounds with trirutile crystal type, such as $NiTa_2O_6$. It needs to be noted that the occupancy data along the [001] direction obtained by refinement of EXAFS function of the material with nominal Ni content of 0.05 need to be taken with care considering overall low Ni concentration and the possible uncertainty of the refined occupancy.

The EXAFS functions of materials with higher Ni content ($x = 0.1$) start to reflect a distortion of the NiO_6 octahedra. The Ni occupancy in the first (the closest) metal−metal coordination shell (i.e., along the *c* axis) changes rather unexpectedly to 0.86 (note that the Ni occupancy of these positions in the material with $x = 0.05$ was equal to zero). The occupancy of Ni in positions of the second metal−metal coordination shell (along the body diagonal) slightly increases from 0.23 to 0.39. This trend can be expected considering an overall increase of Ni concentration. The occupancy numbers resulting from the fit strongly suggest a segregation of most of the Ni ions in a small fraction of the volume of crystallites. The refined Ni−Ni distance along the *c* axis equals 2.94 Å, which is significantly shorter than that of Ru−Ru (3.06 Å). The change in the average bond length has to be seen as an evidence of structural change within Ni clusters, when the ideal rutile lattice cannot be applied for the description of the structure.

A further increase in the Ni content ($x = 0.15$, 0.2, and 0.3) leads to a change of the relative intensity of the peaks corresponding in the EXAFS function to both metal−metal coordination shells. This trend is rather surprising, since already for $x = 0.1$ the corresponding lattice cationic sites along the *c* axis are almost fully occupied with Ni and a further conceivable increase of Ni fraction by ca. 14% cannot explain the almost 3-fold increase in the corresponding peak intensity. A natural explanation of this trend would be a coexistence of Ni-doped RuO_2 phase with an amorphous NiO, which cannot be detected by XRD but which shows up in the EXAFS function. Such a hypothesis seems to be in accordance with rather small variability of the EXAFS functions calculated from Ru K edge data. Nevertheless, as can be seen in Figure 9 the EXAFS functions calculated from the Ni edge absorptions spectra of the materials with relatively high nickel content ($x > 0.15$) fail to reproduce the features characteristic of NiO for distances beyond 4 Å. In other words, the structural motif of NiO disappears already on the length-scale of a single unit cell. Although one may expect the existence of only a short-range order for an amorphous oxide, the absence of the characteristic atomic packing already in the range of one unit cell is unlikely. In addition, an assumption about the presence of the simple oxide cannot explain the higher oxidation state of Ni evident from XPS and XANES data, which seem to correspond to homogeneous materials rather than to multiphase samples.

Therefore, an alternative explanation may involve formation of defects within rutile structure, which localize the incorporated Ni. Such defects would be characterized by the higher metal−metal coordination numbers in the first coordination shell than allowed in the ideal rutile structural model and should most likely resemble the atomic packing of rock-salt-type structure of NiO, at least in the short range. Although this type of defects has never been reported for RuO_2-based oxides, the local atoms packing similar to rock salt type is known for oxygen-deficient titanium oxides, which are derived from isostructural titania polymorph.[37] This defect in the Ru-based system could be described as Ni-rich shear planes propagating along the {121} plane of the crystal. These shear planes are separated by Ru-rich rutile blocks, as shown in Figure 10.

The adequateness of the above-described hypothesis can be verified by refinement of the Ni-EXAFS functions of the $Ru_{1-x}Ni_xO_{2-\delta}$ for $x > 0.10$ using a structural model of shear planes in the oxygen-deficient Ti_nO_{2n-1} phases, e.g., in Ti_9O_{17}.[38] We modified the literature structural data by placing Ni atoms in the corresponding titanium positions in the shear planes and filled the remaining cationic positions with Ru. Taking Ni as a core atom and limiting the cluster size to 4 Å radius, one may construct the defect in the lattice with the architecture presented in Figure 10 as a "rock-salt-type packing". It is worth mentioning that lattice parameters of the ideal TiO_2 rutile ($a = 4.594$ Å, $c = 2.958$ Å) are slightly different from the lattice parameters of RuO_2 conforming to the same structural type ($a = 4.492$ Å, $c = 3.0995$ Å); therefore, one should not expect that the architecture of the Ni-rich defect derived from Ti_9O_{17} to match perfectly the experimental EXAFS function. Nevertheless, after isotropic expansion of cluster during the first stage of the refinement, the theoretical curve reproduces the important

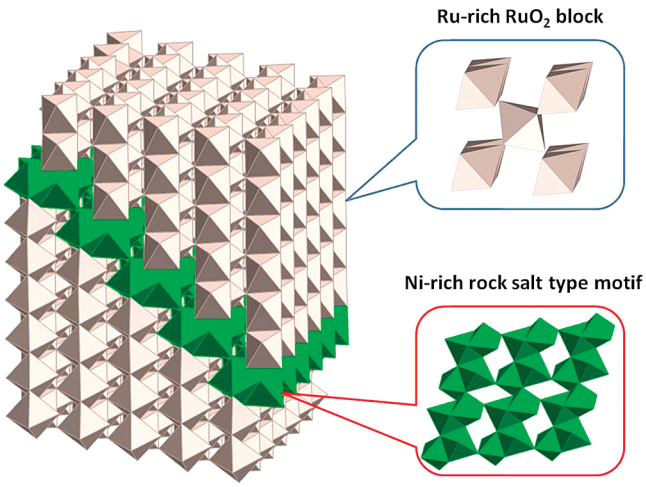

Figure 10. Proposed structural model based on the EXAFS data for $Ru_{1-x}Ni_xO_{2-\delta}$ oxides with $x > 0.10$.

features of the observed experimental curve in an acceptable way with the value of R factor = 0.08. Further improvement of the fit was achieved after metal−metal bond distances were allowed to vary independently, and the result of the final circle of the refinement is shown in Figure 9b ($x = 0.30$). The refined interatomic distances are summarized in Table 2b. To minimize the number of refined parameters the first Ni−O coordination shell was allowed to change isotropically starting from the atomic arrangement of Ti_9O_{17}. The refined metal−oxygen distances are, therefore, probably subject to a large error and need to be taken with care. The interatomic distances in the metal−metal coordination shells, which are more important from the point of view of structural model formulation for this particular type of defect cluster, are more reliable. The results shown in Figure 9b for $x = 0.30$ composition and in Table 2b can be taken as a confirmation of the proposed model of Ni clustering.

The idea of the Ni-rich shear-plane-like defects within RuO_2 host has several consequences. First of all, it addresses the problem of expected oxygen deficiency, which follows from the proposed chemical composition and which is supported by XPS and XANES data. The oxygen deficiency resulting from the oxidation state of Ni being lower than +4 may either lead to formation of vacancies in the oxygen sublattice or may be compensated by local structural rearrangement. The available data do not confirm substantial formation of lattice vacancies. The formation of shear-plane-like defects in $Ru_{1-x}Ni_xO_{2-\delta}$ oxides, on the other hand, is intrinsically connected with oxygen substoichiometry near the Ni ions. In this respect, the proposed model represents a way to accommodate lower-valent cations in the structure and maintain the electroneutrality condition without the need to create lattice oxygen vacancies.

In fact, a similar mechanism, i.e., a formation of {121} sheer planes, was observed in structurally similar Ti_nO_{2n-1} (so-called Magneli phases), where one needs to accommodate for the presence of trivalent titanium in the structure.[38] It is known that the limiting composition of Magneli phases corresponds to $TiO_{1.75}$. Although the oxygen content ($2-\delta$) estimate based on the average oxidation state of Ni and Ru and on the electroneutrality requirement is rather speculative, the application of this approach for material with $x = 0.3$ (where the average oxidation state of Ni is the closest to +2) yields the composition $Ru_{0.7}Ni_{0.3}O_{1.7}$ (i.e., $\delta = 0.3$). This composition is rather close to that of the terminal composition of Magneli phases. This agreement allows one to suggest the shear plane formation to be the prevalent mechanism to accommodate the oxygen deficiency of (i.e., formally partially reduced) oxides based on rutile structural type regardless of the nature of the transition metal forming the rutile structure. The ratio of the metal and oxygen (1:1.7) reflects the limit of the structure to compensate for the oxygen nonstoichiomentry, and in this respect, it also limits the solubility of the Ni in the lattice of RuO_2.

Second, it reconciles the observed trends in XANES spectra, where one observes a shift of the edge position with increasing Ni content in Ni edge data and basically the same edge position for all samples on Ru edge. The weak dependence of the Ru K edge position on the total Ni content supports the proposed localization of the Ni in a relatively small volume when the number of Ru atoms affected by the presence of the Ni remains small. Moreover, the resulting oxygen stoichiometry compensates for the change of the overall positive charge. As a result, the average oxidation state of Ru remains constant and does not affect the edge position. The Ni edge XANES data then reflect two factors: (i) the increasing Ni−Ni interactions when the Ni distribution in the material starts to shift from small clusters [featuring two to three Ni atoms along the [111] direction] to shear-plane-like inclusions protruding along the [121] direction for Ni contents of 0.1 and higher and (ii) the difference in the electronic state of Ni ions located in Ru sites of normal rutile lattice and in the Ni-rich blocks with rock-salt-like packing.

The structural model based on EXAFS data is essentially a consistent description of the Ni distribution in the bulk of the prepared materials; therefore, its relevance to the rationalization of electrocatalytic activity, which is controlled by the surface structure, seems to be relatively weak. It has to be noted, however, that the surface structure of nanocrystalline materials is difficult to assess directly. Despite being of bulk character, the EXAFS data provide the essential structural model needed to address the electronic structure of the $Ru_{1-x}Ni_xO_{2-\delta}$ materials mainly for the stable phases with $x \leq 0.1$. This relationship seems to be missing for the materials with $x > 0.1$, where a measurable Ni dissolution occurs.

It can be easily envisaged that the Ni remains stable in acid media only stabilized by RuO_2 host. Assuming that the shape of the nanocrystals of $Ru_{1-x}Ni_xO_{2-\delta}$ will be similar to that common for rutile structural type, we can expect that the localized Ni can be exposed to corrosive solution either as a line defect on (101), (111), and (100) faces or it may form the whole faces on the prismatic part of nanocrystals.[6] The probability of two-dimensional exposure on the crystal faces increases with increasing Ni content; hence, one should expect lower corrosion stability of the materials with high Ni content. As follows from the EXAFS-based structural model, such a selective Ni dissolution leads to an exposure of surfaces that are not present on usual rutile-type crystal, the electrocatalytic activity of which may be quite different from that of conventional rutile-type surfaces.

Keeping in mind that deviation of the proposed structural model from defect-free rutile is connected only with the presence of the Ni-rich regions, one might view the shear-plane-like defects (and their immediate Ru neighbors) or their protrusion on the surface as the primary sites of the electrocatalytic activity in oxygen or chlorine evolution reaction.

Conclusions

Energy dispersed X-ray spectroscopy (EDX), X-ray photoelectron spectroscopy (XPS), and X-ray absorption spectroscopy (XAS) in XANES and EXAFS modes were implemented to

gather the structural information relevant to the electrocatalytic behavior of nanocrystalline $Ru_{1-x}Ni_xO_{2-\delta}$ oxides. The XRD analysis identifies all samples as single phase, and the EDX data indicated that Ni concentrations in the prepared materials agree with the target composition of $Ru_{1-x}Ni_xO_{2-\delta}$ ($x = 0.0$, 0.05, 0.10, 0.15, 0.20, and 0.3). The EDX data also show that the $Ru_{1-x}Ni_xO_{2-\delta}$ samples are stable in acid media under anodic polarization as long as the $x \leq 0.10$. For the materials with higher nominal Ni content, there is a selective Ni leaching under conditions of electrocatalytic experiments.

Regardless of the actual bulk Ni content, XPS data show an enrichment of the surface of the $Ru_{1-x}Ni_xO_{2-\delta}$ oxides by Ni with respect to projected stoichiometry. The Ni surface "over-stoichiometry" is not affected during the electrocatalytic experiments. A conservative interpretation of the Ru 3d, Ni 2p, and O 1s photoelectron spectra suggests that the majority of surface-confined ruthenium is present in the tetravalent state as Ru^{4+}, while the Ni exists predominantly as Ni^{2+} with an admixture of Ni^{3+}.

The XANES results conform to those obtained by XPS. The Ru K edge data identify Ru^{4+} as the prevailing bulk oxidation state of Ru in the system; the average oxidation state of Ni determined from Ni K edge position agrees with the distribution of Ni between oxidation states of +2 and +3 with trivalent nickel being more populated in materials with low nominal Ni content.

The EXAFS part of the X-ray absorption spectra shows in the case of Ru K edge data that the preferred local environment of Ru in the $Ru_{1-x}Ni_xO_{2-\delta}$ oxides conforms to that observed in idealized RuO_2. The local environment of Ni extracted from Ni K edge spectra is more deviated from that common in the rutile structure. The refinement of the EXFAS functions indicates a strong tendency of the Ni to form clusters within the rutile framework. The formation of the clusters initially starts with a preferred Ni−Ni distance of ca. 3.5 Å, but from $x = 0.10$ changes for preferred Ni−Ni distance of ca. <3.1 Å. This leads eventually to the formation of Ni-rich defects with local structure around Ni ions similar to that of shear planes in the oxygen-deficient rutile phases. Keeping in mind that formation of Ni-rich defects with the rock-salt-type atomic packing is the only feature that distinguished $Ru_{1-x}Ni_xO_{2-\delta}$ oxides from Ni-free RuO_2, most likely it is the Ni-rich defects with shear-plane-like structure that act as the primary sites of the electrocatalytic activity in oxygen or chlorine evolution reaction.

Acknowledgment. This work was supported by the Grant Agency of the Academy of Sciences of the Czech Republic under contract No. IAA400400906. V.P. acknowledges the support of the Marie Curie International Incoming Fellowship (IIF No. 220711) of the European Commission. The synchrotron measurement time was provided by KEK (Tsukuba, Japan) within the research project No. 2008P008. The authors thank Prof. Yasuhiro Inada (Ritsumeikan University) for guidance and useful suggestions on data collection at the synchrotron facility.

Supporting Information Available: Information as noted in the text. This material is available free of charge via the Internet at http://pubs.acs.org.

References and Notes

(1) Rossmeisl, J.; Qu, Z. W.; Zhu, H.; Kroes, G. J.; Norskov, J. K. *J. Electroanal. Chem.* **2007**, *607*, 83.

(2) Wohlfahrtmehrens, M.; Heitbaum, J. *J. Electroanal. Chem.* **1987**, *237*, 251.

(3) Fierro, S.; Nagel, T.; Baltruschat, H.; Comninellis, C. *Electrochem. Commun.* **2007**, *9*, 1969.

(4) Willsau, J.; Wolter, O.; Heitbaum, J. *J. Electroanal. Chem.* **1985**, *195*, 299.

(5) Jirkovsky, J.; Makarova, M.; Krtil, P. *Electrochem. Commun.* **2006**, *8*, 1417.

(6) Jirkovsky, J.; Hoffmannova, H.; Klementova, M.; Krtil, P. *J. Electrochem. Soc.* **2006**, *153*, E111.

(7) Makarova, M. V.; Jirkovsky, J.; Klementova, M.; Jirka, I.; Macounova, K.; Krtil, P. *Electrochim. Acta* **2008**, *53*, 2656.

(8) Da Silva, L. M.; Boodts, J. F. C.; De Faria, L. A. *Electrochim. Acta* **2001**, *46*, 1369.

(9) Da Silva, L. A.; Alves, V. A.; daSilva, M. A. P.; Trasatti, S.; Boodts, J. F. C. *Electrochim. Acta* **1997**, *42*, 271.

(10) De Faria, L. A.; Boodts, J. F. C.; Trasatti, S. *Colloids Surf. A* **1998**, *132*, 53.

(11) De Faria, L. A.; Trasatti, S. *J. Electroanal. Chem.* **1992**, *340*, 145.

(12) Macounova, K.; Makarova, M.; Franc, J.; Jirkovsky, J.; Krtil, P. *Electrochem. Solid State Lett.* **2008**, *11*, F27.

(13) Macounova, K.; Makarova, M.; Jirkovsky, J.; Franc, J.; Krtil, P. *Electrochim. Acta* **2008**, *53*, 6126.

(14) Macounova, K.; Jirkovsky, J.; Makarova, M. V.; Franc, J.; Krtil, P. *J. Solid State Electrochem.* **2009**, *13*, 959.

(15) Trasatti, S. *Electrochim. Acta* **1987**, *32*, 369.

(16) Trasatti, S. *Electrochim. Acta* **2000**, *45*, 2377.

(17) Neville, M. *J. Synchrotron Radiat.* **2001**, *8*, 322.

(18) Foo, M. L.; Huang, Q.; Lynn, J. W.; Lee, W.-L.; Klimczuk, T.; Hagemann, I. S.; Ong, N. P.; Cava, R. J. *J. Solid State Chem.* **2006**, *179*, 563.

(19) Shirley, D. *Phys. Rev. B* **1972**, *5*, 4709.

(20) Scofield, J. *J. Electron Spectrosc. Relat. Phenom.* **1976**, *8*, 129.

(21) Shannon, R. D. *Acta Crystallogr.* **1976**, *A32*, 751.

(22) Garbasi, F.; Bossi, A.; Petrini, G. *J. Mater. Sci.* **1980**, *15*, '2559.

(23) Gaudet, J.; Tavarez, A. C.; Trasatti, S.; Guay, D. *Chem. Mater.* **2005**, *17*, 1570.

(24) Tsukada, K.; Kameyama, K.; Yahikozawa, K.; Takasu, Y. *Denki Kanagku* **1993**, *61*, 435.

(25) Berlich, A.; Liu, Y. Ch.; Morgner, H. *Radiat. Phys. Chem.* **2005**, *74*, 201.

(26) Paulus, U. A.; Wang, Y.; Kim, S. H.; Geng, P.; Winterlin, J.; Jacobi, K.; Ertl, G. *J. Chem. Phys.* **2004**, *121*, 11301.

(27) Kotz, R.; Lewerenz, H. J.; Stucki, S. *J. Electrochem. Soc.* **1983**, *130*, 825.

(28) Lewerenz, H. J.; Stucki, S.; Kotz, R. *Phys. Rev. B* **1983**, *126*, 893.

(29) Foelske, A.; Barbieri, O.; Hanhn, M.; Kotz, R. *Electrochem. Solid State Lett.* **2006**, *9*, A268.

(30) Over, M.; Seivtsonen, A. P.; Lundgren, E.; Smedh, M.; Andersen, J. N. *Surf. Sci.* **2002**, *504*, L196.

(31) Froment, P.; Genet, M. J.; Devillers, M. *J. Electron Spectrosc. Relat. Phenom.* **1999**, *104*, 119.

(32) Grosvenor, A. P.; Beisinger, M. C.; Smart, R.; St, C.; McItyre, N. S. *Surf. Sci.* **2006**, *600*, 1771.

(33) Gupta, R. P.; Sen, S. K. *Phys. Rev. B* **1974**, *10*, 71–77.

(34) Grosvenor, A. P.; Biesinger, M. C.; Smart, R. S.; McIntyre, N. S. *Surf. Sci.* **2006**, *600*, 1771.

(35) Rochefort, D.; Dabo, P.; Guay, D.; Sherwood, P. M. A. *Electrochim. Acta* **2003**, *48*, 4254.

(36) McKeown, D. A.; Hagans, P. L.; Carette, L. P. L.; Russell, A. E.; Swider, K. E.; Rolison, D. R. *J. Phys. Chem. B* **1999**, *103*, 4825.

(37) Rao, C. N. R.; Gopalkrishnan, J. *New Directions in Solid State Chemistry*; Cambridge University Press: New York, 1997.

(38) LePage, Y.; Strobel, P. *J. Solid State Chem.* **1982**, *44*, 273–281.

JP904935E